

Gamma-ray observations of the Be/pulsar binary 1A 0535+262 during a giant X-ray outburst

V. A. Acciari¹, E. Aliu², M. Araya³, T. Arlen⁴, T. Aune⁵, M. Beilicke⁶, W. Benbow¹, S. M. Bradbury⁷, J. H. Buckley⁶, V. Bugaev⁶, K. Byrum⁸, A. Cannon⁹, A. Cesarini¹⁰, L. Ciupik¹¹, E. Collins-Hughes⁹, W. Cui^{3,†}, R. Dickherber⁶, C. Duke¹², A. Falcone¹³, J. P. Finley³, L. Fortson¹¹, A. Furniss⁵, N. Galante¹, D. Gall³, S. Godambe¹⁴, S. Griffin¹⁵, R. Guenette¹⁵, G. Gyuk¹¹, D. Hanna¹⁵, J. Holder¹⁶, G. Hughes²¹, C. M. Hui¹⁴, T. B. Humensky¹⁷, A. Imran¹⁸, P. Kaaret¹⁹, M. Kertzman²⁰, H. Krawczynski⁶, F. Krennrich¹⁸, A. S. Madhavan¹⁸, G. Maier^{21,†}, P. Majumdar⁴, S. McArthur⁶, P. Moriarty²², R. A. Ong⁴, A. N. Otte⁵, D. Pandel¹⁹, N. Park¹⁷, J. S. Perkins¹, M. Pohl²³, H. Prokoph²¹, J. Quinn⁹, K. Ragan¹⁵, L. C. Reyes¹⁷, P. T. Reynolds²⁴, E. Roache¹, H. J. Rose⁷, D. B. Saxon¹⁶, G. H. Sembroski³, G. Demet Senturk²⁵, A. W. Smith⁸, G. Tešić¹⁵, M. Theiling¹, S. Thibadeau⁶, A. Varlotta^{3,†}, S. Vincent¹⁴, M. Vivier¹⁶, S. P. Wakely¹⁷, J. E. Ward⁹, T. C. Weekes¹, A. Weinstein⁴, T. Weisgarber¹⁷, S. Weng³, D. A. Williams⁵, M. Wood⁴, B. Zitzer³

¹Fred Lawrence Whipple Observatory, Harvard-Smithsonian Center for Astrophysics, Amado, AZ 85645, USA

²Department of Physics and Astronomy, Barnard College, Columbia University, NY 10027, USA

³Department of Physics, Purdue University, West Lafayette, IN 47907, USA; avarlott@purdue.edu, cui@purdue.edu

⁴Department of Physics and Astronomy, University of California, Los Angeles, CA 90095, USA

⁵Santa Cruz Institute for Particle Physics and Department of Physics, University of California, Santa Cruz, CA 95064, USA

⁶Department of Physics, Washington University, St. Louis, MO 63130, USA

⁷School of Physics and Astronomy, University of Leeds, Leeds, LS2 9JT, UK

⁸Argonne National Laboratory, 9700 S. Cass Avenue, Argonne, IL 60439, USA

⁹School of Physics, University College Dublin, Belfield, Dublin 4, Ireland

¹⁰School of Physics, National University of Ireland Galway, University Road, Galway, Ireland

¹¹Astronomy Department, Adler Planetarium and Astronomy Museum, Chicago, IL 60605, USA

¹²Department of Physics, Grinnell College, Grinnell, IA 50112-1690, USA

¹³Department of Astronomy and Astrophysics, 525 Davey Lab, Pennsylvania State University, University Park, PA 16802, USA

¹⁴Department of Physics and Astronomy, University of Utah, Salt Lake City, UT 84112, USA

¹⁵Physics Department, McGill University, Montreal, QC H3A 2T8, Canada

¹⁶Department of Physics and Astronomy and the Bartol Research Institute, University of Delaware, Newark, DE 19716, USA

¹⁷Enrico Fermi Institute, University of Chicago, Chicago, IL 60637, USA

¹⁸Department of Physics and Astronomy, Iowa State University, Ames, IA 50011, USA

¹⁹Department of Physics and Astronomy, University of Iowa, Van Allen Hall, Iowa City, IA 52242, USA

²⁰Department of Physics and Astronomy, DePauw University, Greencastle, IN 46135-0037, USA

²¹DESY, Platanenallee 6, 15738 Zeuthen, Germany; gernot.maier@desy.de

²²Department of Life and Physical Sciences, Galway-Mayo Institute of Technology, Dublin Road, Galway, Ireland

²³Institut für Physik und Astronomie, Universität Potsdam, 14476 Potsdam-Golm, Germany

²⁴Department of Applied Physics and Instrumentation, Cork Institute of Technology, Bishopstown, Cork, Ireland

²⁵Columbia Astrophysics Laboratory, Columbia University, New York, NY 10027, USA

ABSTRACT

Giant X-ray outbursts, with luminosities of about 10^{37} erg s⁻¹, are observed roughly every 5 years from the nearby Be/pulsar binary 1A 0535+262. In this article, we present observations of the source with VERITAS at very-high energies (VHE; $E > 100$ GeV) triggered by the X-ray outburst in December 2009. The observations started shortly after the onset of the outburst, and they provided comprehensive coverage of the episode, as well as the 111-day binary orbit. No VHE emission is evident at any time. We also examined data from the contemporaneous observations of 1A 0535+262 with the Fermi/LAT at high energy photons (HE; $E > 0.1$ GeV) and failed to detect the source at GeV energies. The X-ray continua measured with the Swift/XRT and the RXTE/PCA can be well described by the combination of blackbody and Comptonized emission from thermal electrons. Therefore, the gamma-ray and X-ray observations suggest the absence of a significant population of non-thermal particles in the system. This distinguishes 1A 0535+262 from those Be X-ray binaries (such as PSR B1259–63 and LS I +61°303) that have been detected at GeV–TeV energies. We discuss the implications of the results on theoretical models.

Subject headings: acceleration of particles - binaries: general - gamma rays: observations - individual (1A 0535+262)

1. Introduction

High-mass X-ray binaries are binary systems in which the mass of the secondary star exceeds 10 solar masses. The majority are Be/X-ray binaries (BeXRBs), consisting of a Be or O star and a neutron star (Liu et al. 2006). Some of the BeXRBs manifest themselves observationally as X-ray pulsars. Be or Oe stars are known to be rapid rotators, so their winds are concentrated strongly around the equatorial plane, forming a circumstellar disk (see review by van Paradijs & McClintock (1995)). The binary orbits of BeXRBs tend to be quite wide and eccentric, with orbital periods typically exceeding 20 days.

BeXRBs are complex systems. They exhibit flux variability over a wide range of wavelengths. The variability can be regular, often correlated with the orbital movement of the

[†]Authors to whom any correspondence should be addressed.

neutron star around the OBe star, or in sudden and strong outbursts. The orbital modulation may be caused by: the varying geometry of the binary system, changes in the physical conditions of the circumstellar disk of the Be star, or the occasional formation of an accretion disk around the compact object. Normal (or Type I) outbursts, with luminosities of $< 10^{37}$ erg s $^{-1}$, are thought to occur when the neutron star in a BeXRB passes through the circumstellar disk (near periastron) and thus accretes at a higher rate (Reig 2007). Giant (or Type II) outbursts occur more rarely but may be seen at any orbital phase, with X-ray luminosities close to the Eddington limit; they are thought to be associated with the formation of a transient accretion disk (Stella et al. 1986).

Recently, several high-mass X-ray binaries have been seen to emit photons in the very-high energy range. Among them, PSR B1259–63/LS 2883 (Aharonian et al. 2005a) and LS I +61°303 (Albert et al. 2006; Acciari et al. 2008) are BeXRBs and are thought to have circumstellar disks. A third VHE source, HESS J0632+057, may also fall in this VHE binary class (Aharonian et al. 2004; Hinton et al. 2009; Acciari et al. 2009). The production of VHE gamma rays can be envisioned in both leptonic and hadronic scenarios. Leptonic models postulate that the interaction between pulsar wind and stellar wind may result in the formation of a strong shock that could accelerate electrons to relativistic energies and that the relativistic electrons may produce VHE gamma rays by upscattering ambient photons. In hadronic scenarios (e.g. Romero et al. (2001) and Orellana & Romero (2005)), a hadron beam is accelerated in the magnetosphere of a neutron star. It impacts the transient accretion disk and produces VHE gamma rays via the decay of neutral pions produced in pp-interactions, a mechanism first proposed by Cheng & Ruderman (1989, 1991).

VHE gamma rays are expected to interact with ambient photons to produce e^+e^- pairs, leading to orbital modulation of the VHE gamma-ray flux (Bednarek 1993). During an outburst, the VHE gamma-ray flux would then peak at the beginning or end of the outburst, when thermal emission from the accretion disk is at a minimum; the system is opaque to gamma rays near the peak of the outburst (Romero et al. 2001; Orellana et al. 2007). In hadronic scenarios, the gamma-rays emitted by the secondary electrons and positrons that are produced in electromagnetic cascades may contribute to fluxes in the MeV to GeV range.

1A 0535+262 has been extensively observed over the years, due to the many giant and minor outbursts that have occurred. The pulsar shows evidence for three representative X-ray intensity states, one of quiescence with a flux level of $\lesssim 10$ mCrab, a normal outburst with a flux level of ~ 10 mCrab to 1 Crab, and a giant outburst with a flux level of several Crab (Kendziorra et al. 1994). Giant outbursts have been observed in April 1975 (Rosenberg et al. 1975), October 1980 (Estulin et al. 1981), June 1983 (Sembay et al. 1990), March/April 1989 (Makino et al. 1989), February 1994 (Finger et al. 1996), May/June 2005 (Caballero et

al. 2007a) and December 2009 (Wilson-Hodge et al. 2010). Studies have been conducted on recent minor outbursts as well (Naik et al. 2008; Caballero et al. 2010). An extensive review of the system was provided by Giovannelli & Graziati (1992).

The Be/X-ray binary 1A 0535+262 has been associated with the EGRET unidentified gamma-ray source 3EG J0542+2610 (Romero et al. 2001) and has therefore long been considered as an object of interest for VHE gamma-ray observations. At a distance of about 2 kpc, 1A 0535+262 is among the closest binary systems (Steele et al. 1998). It consists of a pulsar of period 103 s in an eccentric orbit ($e = 0.47$) with an O9.7-B0 IIIe star. The orbital period is 111 days (Coe et al. 2006). X-ray observations of 1A 0535+262 may suggest the formation of a transient accretion disk during giant outbursts (Finger et al. 1996). Figure 1 shows a long-term X-ray light curve of 1A 0535+262, as measured with the All-Sky Monitor (ASM) on board the *Rossi X-ray Timing Explorer* (RXTE), over a period of roughly 15 years. The presence of both normal and giant outbursts is clearly seen. The December 2009 outburst peaked around 1.3 Crab (95 ASM counts s^{-1}) and it is second only to the May/June 2005 outburst peak (1.7 Crab, 120 counts s^{-1}). The outburst duration, ~ 40 days, the X-ray flux intensity (peak intensity greater than the Crab) and the occurrence of the outburst at a random binary phase are all in line with a representative Type II outburst event.

In this article we report on X-ray and gamma-ray observations of 1A 0535+262 during a giant outburst in December 2009 (as shown in Fig. 1). During the outburst, the hard X-ray (15-50 keV) flux, as measured with the Burst Alert Telescope (BAT) on board the *Swift Gamma Ray Burst Mission* (Swift), reached a level of >5 times that of the Crab Nebula. Triggered by the alerts from the Swift/BAT, the VHE gamma-ray observatory, the *Very Energetic Radiation Imaging Telescope Array System* (VERITAS), monitored 1A 0535+262 for a full orbital period (see Fig. 2). These data are complemented by observations in soft X rays with the X-ray Telescope (XRT) on Swift, in hard X rays with the Proportional Counter Array (PCA) on RXTE, and in GeV gamma rays with the Large Area Telescope (LAT) on *Fermi Gamma Ray Space Telescope*.

2. Observations

2.1. VERITAS: VHE Gamma-Ray Observations

VERITAS is a ground-based gamma-ray telescope array located at the Fred Lawrence Whipple Observatory in southern Arizona (1.3 km above sea level, N31° 40', W110° 57'). It consists of four 12-meter imaging Cherenkov telescopes with 499-pixel cameras, designed to detect the faint flashes of Cherenkov light from air showers initiated in the atmosphere by

high-energy photons. VERITAS is sensitive to photons in the energy range from 100 GeV to 30 TeV, with a maximum effective area of approximately 10^5 m^2 . At 1 TeV the angular resolution is better than 0.1° and the energy resolution is 15-20%. The field of view of the VERITAS telescopes is 3.5° . The observatory was upgraded in summer 2009, leading to a sensitivity sufficient to detect sources with a flux of 1% of the Crab Nebula in less than 30 hours of observations (1 h for 5% of the Crab Nebula flux). Observations with VERITAS are possible during dark-sky and moderate moonlight conditions (the moon less than 50% illuminated). Elevated background light levels during moderate moonlight lead to a lower sensitivity to gamma rays at the threshold. For more details on the VERITAS instrument, see e.g. Acciari et al. (2008).

VERITAS observed 1A 0535+262 for 30 hours. 23 hours 40 minutes remain after the application of quality-selection criteria, which remove data taken during bad weather or affected by hardware-related problems. For some observations only three telescopes were operational (missing telescope 4 on 2009 December 24 and 2010 February 10), leading to a moderately reduced sensitivity during these periods. The triggering criterion (a counting rate of $>0.1 \text{ counts s}^{-1}$ reported by the Swift/BAT instrument) for observations of flaring X-ray binaries with VERITAS was fulfilled on 2009 December 5 (Wilson-Hodge et al. 2010). Observations started on 2009 December 6, shortly after the beginning of the giant flare. They were delayed by one day due to very bright moonlight conditions. The observation covered most of the flare, included the apastron phase, and continued for almost 90 days until the following periastron phase. Table 1 shows the daily observation log, including weather condition, elevation range and moonlight condition. Figure 2 (right) shows the relative orbit of 1A 0535+262 around the Be companion star.

The analysis steps consist of calibration, image cleaning, second-moment parameterization of the recorded images (Hillas 1985), reconstruction of shower direction and impact parameter using stereoscopic methods (see e.g. Krawczynski et al. (2006)), gamma-ray/hadron separation and the generation of sky maps. Images in at least three cameras are required; additional cuts on the shape of the event images and direction of the primary particles are used to reject the far more numerous background events. These cuts are optimized for a 5% Crab Nebula flux source. The energy threshold after analysis cuts is 220 GeV at a 10° zenith angle and 450 GeV at a 40° zenith angle and the systematic error on the energy estimation of the primary gamma rays is about 20%. The data were taken in wobble mode (Fomin et al. 1994), wherein the object was positioned at a fixed offset of 0.5° in one of four directions from the camera center. The search region for photons from the putative gamma-ray source is defined by a 0.1° radius circle centered on the position of the Be star in 1A 0535+262 (Perryman et al. 1997). The background in the source region is estimated from the same field of view using the ring-background model with a ring size of 0.5° (mean

radius) and a ring width of 0.1° (Aharonian et al. 2005b). In order to reduce systematic errors in the background estimation, regions around stars with B magnitudes brighter than 6 are excluded.

2.2. Fermi LAT: High-Energy Gamma-Ray Observations

Fermi was placed in orbit on 2008 June 11 and has been acquiring data primarily in all-sky survey mode since 2008 August 4. It carries on board two science instruments: the *Gamma-ray Burst Monitor* (GBM) and the *Large Area Telescope* (LAT). For this work we only used data from the LAT, which is sensitive to high energy photons (HE; $E > 0.1$ GeV). The LAT is an e^+e^- pair production telescope containing solid-state silicon trackers and cesium iodide calorimeters, which are sensitive to photons in the energy range from ~ 20 MeV to ~ 300 GeV. It has a field of view of ~ 2.4 sr, an on-axis effective area of ~ 8000 cm² for energies $\gtrsim 1$ GeV, and an angular resolution (for 68% containment at 1 GeV) better than 1° (Atwood et al. 2009).

For this work we used data from LAT observations of 1A 0535+262 that were conducted between 2009 November 30 and 2010 February 22. We used the Fermi Science Tools v9r15p2 software analysis package to reduce the data and followed the event selection recommendations from the Fermi Science Support Center¹. Briefly, we selected photons from the Pass 6 diffuse class events, those that have the highest probability of being gamma rays, with the `gtselect` tool. In order to avoid contamination from Earth albedo photons, time periods when the region around 1A 0535+262 was observed at zenith angles greater than 105° were eliminated from further analysis. We also limited the spectral range to above 200 MeV to reduce contamination by the galactic diffuse gamma-ray background.

At low energies, the point spread function (PSF) of the LAT is quite large, so it was necessary to deal with contamination by potential sources in the vicinity of 1A 0535+262. For this reason, a circular region of interest (RoI), centered on 1A 0535+262, was chosen with a radius of 8.5° . We chose a source region of radius 17° , also centered on 1A 0535+262, that encompasses the supernova remnant IC 443, which is 9.5° from 1A 0535+262, and the Geminga pulsar, which is 15.3° away. Both of these sources are known GeV-TeV gamma-ray emitters. IC 443 and Geminga were modeled as described by Abdo et al. (2010a) and Abdo et al. (2010b), respectively. All sources in the 11-month Fermi LAT catalog (Abdo et al. 2010c) inside the source region were considered. The catalog consists of data acquired from 2008 August 4 to 2009 July 4, which in the case of 1A 0535+262 contains data over

¹<http://fermi.gsfc.nasa.gov/ssc/data/analysis/scitools/>

several orbital periods but before the giant December 2009 outburst. There is no detection for 1A 0535+262 in the catalog. 1A 0535+262 is modeled assuming a fixed spectral index of 2.1 while the normalization is left as a free parameter. The sources were assumed to have a power-law spectrum, which was derived from the fluxes in the Fermi LAT catalog.

Two differences from the 11-month catalog were encountered during the analysis. First, the source 1FGL J0623.5+3330 possessed a test statistic (TS) value ten times higher than that reported in the Fermi catalog (see Mattox et al. (1996) for further information on the test statistic). To account for such variability, we left both the normalization and spectral index free. Second, an unidentified source was also found at the position RA 74.12° and Dec 26.99° with a TS value of 68, and it was included in the source model. The spectral parameters were allowed to vary during the fit for sources that lie within the RoI but were fixed for those outside of the RoI (but still inside of the source region). An improvement to the source model fit was achieved when IC 443, which is in the source region, was allowed to vary with free model parameters. Besides discrete sources, contamination by the diffuse background was also taken into account. The galactic and extragalactic backgrounds were represented with *gll_iem_v02.fit* and with a power-law model of index 4.09, respectively. The instrument response function (IRF) used in this analysis is IRF P6_V3_DIFFUSE.

2.3. Swift/XRT: X-Ray Observations

Swift is a gamma-ray burst satellite that contains three scientific instruments on board: the *Burst Alert Telescope* (BAT), the *X-ray Telescope* (XRT), and the *UV/Optical Telescope* (UVOT). With a field of view of 2 sr, the BAT is an effective hard X-ray sky monitor. The detailed studies presented in this work relied on data from the XRT. The XRT operates in the 0.3-10 keV band. It consists of a focusing X-ray telescope and CCD detectors at the focal plane (Burrows et al. 2004).

Triggered by alerts from the BAT, 1A 0535+262 was observed with the XRT between 2009 December 7 and December 27. Table 2 provides a summary of the observations. Due to the brightness of the source, the Windowed Timing (WT) mode (Capalbi et al. 2005) was adopted to minimize the effects of photon pile-up. The XRT data were reduced and analyzed with FTOOLS in the HEASOFT package version 6.5.² For each observation, initial event filtering and selection was carried out using the `xrtpipeline` script, with standard quality cuts, and only events with grades 0-2 were selected as good events. Source counts were extracted, with `xselect`, from a 20 × 60 pixel rectangular box centered on 1A 0535+262,

²<http://heasarc.gsfc.nasa.gov/docs/software/lheasoft/>

while background counts were taken from a rectangular region of the same size outside of the source region. An exposure map was generated with `xrtexpomap` and was used to correct for bad columns. Finally, source and background spectra were constructed. The spectra were grouped to contain a minimum of 100 counts per bin and a 1% systematic error was added to the data (Steiner et al. 2010). To facilitate subsequent spectral analyses, an ancillary response file (`arf`) was produced with `xrtmkarf`, to go along with the adopted response matrix (`swxwt0to2s0_20010101v011.rmf`).

Even in the Windowed Mode, event pile-up was significant in some observations. For instance, near the peak of the outburst (on 2009 December 8), the pile-up of photons reached about 11%. Therefore, the effects need to be properly accounted for. We adopted a procedure similar to that of Romano et al. (2006) to correct the pile-up effects. Briefly, for each observation, we constructed an X-ray spectrum by excluding a central region of the source. We varied the size of the exclusion box until the spectrum was stabilized (based on the results of spectral fitting). After the procedure, the remaining pile-up effects on the spectrum are expected to be minimal.

2.4. RXTE/PCA: X-Ray Observations

Besides the ASM, RXTE carries two pointed instruments: the *Proportional Counter Array* (PCA) and the *High Energy X-ray Timing Experiment* (HEXTE). For this work only data from the PCA were employed. The PCA was designed to cover an energy range of 2.0–60.0 keV and consists of five, nearly identical, large-area xenon proportional counter units (PCUs). The field of view is about $1^\circ \times 1^\circ$. Each PCU has an area of $\sim 1300 \text{ cm}^2$, for a total effective area of 6500 cm^2 (Jahoda et al. 1996). Operational constraints often require that some of the PCUs be turned off, but PCU 2 was always in operation for our observations during the outburst.

1A 0535+262 was observed by RXTE between 2009 December 4 and 2010 January 4. Table 3 shows an observation log. We reduced the data using FTOOLS in the HEASOFT package (version 6.5)³. The PCA has numerous data modes, and multiple modes are usually employed in an observation. For this work, however, we only used the *Standard 2* data. For a given observation, we first filtered data by following the standard procedure⁴, which resulted in a list of good time intervals (GTIs). We then simulated background events for the

³<http://heasarc.gsfc.nasa.gov/docs/software/lheasoft/>

⁴See the online RXTE Cook Book at http://heasarc.gsfc.nasa.gov/docs/xte/recipes/cook_book.html

observation by using the latest background model (*pca_bkgd_cmbrightvle_eMv20051128.mdl*) that is appropriate for bright sources. Using the GTIs, we proceeded to make a spectrum for PCU 2 by using data from only the first xenon layer (which is most accurately calibrated), which limits the spectral coverage to below 25–30 keV. Since few counts were detected at higher energies, the impact of the reduced spectral coverage was very minimal. The selected energy range is below the range where 1A 0535+262 produces cyclotron lines, which are due to the first and second harmonic cyclotron absorption at ~ 45 keV and ~ 100 keV (Kendziorra et al. 1994; Caballero et al. 2007b). We repeated the steps to derive a corresponding background spectrum for PCU 2 from the simulated events. We added 1% systematic uncertainty to the spectra for subsequent spectral modeling to account for the uncertainty in the instrumental response (Jahoda et al. 2006).

3. Results

3.1. VERITAS

Analysis results for the combined VERITAS data set can be found in Table 4. Figure 3 shows the region of the sky around 1A 0535+262 as seen by VERITAS. No evidence for VHE gamma rays has been found. The flux upper limit at the 99% confidence level (Helene 1983) assuming a power-law-like source spectrum with a spectral index of $\Gamma = 2.5$ is $F(> 0.3 \text{ TeV}) < 0.5 \times 10^{-12} \text{ ph cm}^{-2} \text{ s}^{-1}$ (about 0.4% of the flux of the Crab Nebula above 0.3 TeV).

The data were arranged in different periods, as gamma-ray production and absorption is expected to vary with orbital movement and flaring state. The four periods are: rising portion and falling portion of the giant flare, apastron and periastron. No VHE emission has been detected in any of these periods; upper limits between 0.9 and 2.0% of the flux of the Crab Nebula ($> 0.3 \text{ TeV}$) have been derived. For details, see Table 4.

3.2. Fermi

A search for HE gamma-ray emission from 1A 0535+262 was performed for a period that spans the onset of the X-ray outburst to the successive apastron of the pulsar (2009 November 30 – 2010 February 22). No significant gamma-ray excess was seen for the same time intervals used for the VERITAS data analysis. We derived a flux upper limit of $F(> 0.2 \text{ GeV}) < 1.9 \times 10^{-8} \text{ ph cm}^{-2} \text{ s}^{-1}$ at the 99% confidence level. To facilitate a comparison with theoretical models, we also derived flux upper limits for different periods of the X-ray outburst (rising and decaying portions) and around apastron and periastron passages. The

results are summarized in Table 5.

3.3. Swift/XRT

The XRT spectrum for each time interval was modeled in XSPEC version 12.6.0k. We used response matrix file (`rmf`) v011, along with the `arf` that we made. During spectral fitting, we limited the energy range to 0.6–10.0 keV, to avoid complicated calibration issues at the lower energies. We should note the presence of two absorption features, at 1.8 and 2.2 keV, respectively, which are probably of instrumental origin as they lie near the Si K and Au M edges.⁵ They were modeled with inverted Gaussians at fixed energies in the spectral modeling.

We fitted the spectra with a model that consists of a blackbody and a power law, both of which are absorbed by foreground matter in the interstellar medium. Good fits were achieved in all cases. The results are shown in Table 6. Spectral hardening during the rising phase of the X-ray outburst is apparent. The reverse trend is noticeable during the decaying phase. We note that the rising phase corresponds to orbital phases 0.11–0.21 and the decaying phase to orbital phases 0.22–0.36.

3.4. RXTE/PCA

Similarly, we modeled the PCA spectra in XSPEC. We limited the energy range to >3 keV, to avoid calibration issues at lower energies. Due to the lack of sensitivity at low energies, for each observation we fixed the hydrogen column density N_H to 3.0×10^{21} cm⁻², which is fairly representative of the values derived from the Swift/XRT observation (see Table 6). We found that the simple model that had worked well for the Swift/XRT spectra could no longer satisfactorily fit the PCA spectra. Examining the residuals, we noted the presence of a broad feature between 6 and 7 keV, which is likely caused by calibration uncertainty near the Xe L edge, although it could also be partially attributable to a K_α line of neutral or ionized iron. We modeled it with a Gaussian and will not discuss it further. More interestingly, we found that we could achieve good fits to the PCA spectra by introducing a high-energy cut-off.

The roll-over of the spectrum at high energies seems to suggest a physical origin of the

⁵See http://heasarc.gsfc.nasa.gov/docs/heasarc/caldb/swift/docs/xrt/SWIFT-XRT-CALDB-09_v14.pdf

hard X-ray emission in thermal inverse Compton scattering. The broad spectral coverage of the RXTE/PCA allows modeling of the X-ray spectrum with a more physical model. We replaced the empirical power law (with a high-energy cut-off) with the *comptt* model in XSPEC. Table 7 summarizes the results. The fits are all excellent. Due to the lack of sensitivity of the PCA at low energies, however, the seed photon temperatures (kT_s) is not well constrained. This also affects other parameters, such as the normalization of *comptt*, because of the coupling between the spectral components.

3.5. Joint Swift/RXTE Analysis

Ideally we would combine both the Swift/XRT and RXTE/PCA data to constrain all spectral components. Unfortunately there were no simultaneous observations, but there were many sets of observations from both satellites which occurred within the timescale of a day. The average energy flux would vary around $\sim 1 \text{ keV cm}^{-2} \text{ s}^{-1}$ per day during the maximum X-ray outburst. We attempted to model these pairs of Swift/XRT and RXTE/PCA observations jointly, with the understanding that the source could have varied spectrally between the two. To account for possible discrepancy in the overall throughput between the XRT and PCA, we introduced a multiplicative constant to the models. We fixed the constant to unity for the XRT but let it float for the PCA.

We experimented with several physical models to gain further insights into the origin of the observed spectral roll-over at high energies, including thermal Comptonization (*comptt*), thermal Bremsstrahlung (*bremss*), and non-thermal synchrotron (*srcut*), in combination with other spectral components that were used in the modeling of the Swift/XRT and RXTE/PCA data (mainly at lower energies). We were not able to find any acceptable fits when we tied all of the physical parameters in the model for the Swift/XRT and RXTE/PCA observations, but when we untied the blackbody parameters (i.e., let them vary independently for the Swift/XRT and RXTE/PCA observations), we obtained a good fit only with the thermal Comptonization model (for hard X-ray emission). This is perhaps an indication that the source did indeed vary significantly between the two observations and seems to indicate that the hard X rays are likely of thermal origin. Figure 4 shows an example (for the rising portion; see Table 8) of the fits and residuals for cases where the blackbody parameters are tied and untied, respectively. The results are summarized in Table 8.

4. Summary and Discussion

We present observations at X-ray and gamma-ray energies of the Be/pulsar binary 1A 0535+262 during its 2009 giant outburst. The results can be summarized as follows: i) There is no evidence for VHE or HE emission from 1A 0535+262 in the VERITAS and Fermi/LAT observations during the giant outburst and during the subsequent apastron and periastron passages; ii) The X-ray spectra measured with the Swift/XRT and RXTE/PCA are best fitted with a model that consists of blackbody and Comptonized emission from thermal electrons at temperatures of approximately 2 keV and 6 keV, respectively. The optically-thick emission may originate from the accretion disk around the neutron star and perhaps also from the “hot spot” on the neutron star surface. The optical depths for the Compton component are ~ 10 (see Table 4). This emission component may be associated with, e.g., a warm layer of the accretion disk or with the accretion column above the “hot spot”.

The non-detection of 1A 0535+262 at VHE and HE wavelengths may indicate that there is no significant non-thermal particle population in the system. This would imply a thermal origin of the X-ray emission, as opposed to a non-thermal leptonic model, in which X-ray emission is the result of synchrotron radiation from non-thermal electrons. A thermal origin is also supported by the fact that 1A 0535+262 has not been detected at radio wavelengths (Giovannelli & Graziati 1992; Romero et al. 2001), which also suggests the lack of non-thermal electrons, as well as by the OSSE/CGRO observation of the source that saw no significant non-thermal component (Grove et al. 1995).

The upper limits derived from VERITAS observations correspond to a luminosity of $< 0.5\text{--}1.5 \times 10^{33}$ erg s $^{-1}$ (see Table 4), assuming a distance to 1A 0535+262 of 2 kpc. Applying the Cheng and Ruderman mechanism to the source, Orellana et al. (2007) derived a gamma-ray luminosity of about 10^{33} erg s $^{-1}$ at 0.3 TeV at the end of giant outbursts (Orellana et al. 2007), which is very close to our upper limits. The Fermi/LAT flux upper limit over the whole orbit (see Table 5) is already below the theoretical flux prediction of 3.8×10^{-8} ph cm $^{-2}$ s $^{-1}$, which was derived by extrapolating the result of Orellana et al. (2007) to the Fermi/LAT energy range. Therefore, our results begin to place severe constraints on hadronic models as well. We note that the upper limits correspond only to a tiny fraction of the Eddington luminosity of the system. In comparison, the X-ray luminosity of 1A 0535+262 can reach about 10% of the Eddington luminosity.

One of the main interests in 1A 0535+262 stems from the previous EGRET gamma-ray source detection before the February 1994 major X-ray outburst peak. There is no Fermi detection for the EGRET source 3EG J0542+2160, and a 99% confidence level flux upper limit at the source location (RA 85.69°, Dec 26.17°) produces a value of $F(> 0.2\text{GeV}) <$

3.5×10^{-8} ph cm² s⁻¹ (test statistic TS is 1.0), for the same source model settings and energy range used for 1A 0535+262 over the whole orbital period. 1FGL J0538.6+2717, the closest catalog source to 1A 0535+262, is 0.98° away and doesn't overlap with the 95% confidence level location radius of 3EG J0542+2610.

The lack of detectable gamma-ray emission may also be attributed to the attenuation of gamma rays via pair production, because of the presence of a strong radiation field in the binary system at both optical and X-ray wavelengths. The VHE gamma rays should be attenuated mainly by IR photons from the companion (Oe) star and are thus expected to be modulated by the orbital motion (Bednarek 2006). However, quantifying the effects of attenuation is complicated by dramatic changes in the accretion rate that are associated with the giant outburst, since the accretion process could also be a source of IR photons and, more importantly, could power the VHE gamma-ray production. In other words, there is significant degeneracy in the production and attenuation of VHE gamma rays. It is worth noting that the secondary electrons (and positrons) from the pair production process could be a source of gamma rays at MeV–GeV energies (Bednarek 2006). The HE gamma rays can be similarly attenuated, mainly by soft X-ray photons. We therefore do not expect to detect such gamma rays near the peak of the X-ray outburst. However, the fact that 1A 0535+262 is not detected with the Fermi/LAT when the attenuation of HE photons is not expected to be significant seems to indicate a genuine lack of gamma-ray production.

Our results seem to suggest that 1A 0535+262 is inherently different from those Be X-ray binaries that have been detected at GeV–TeV energies, including PSR B1259–63 and LS I +61°303, in terms of gamma-ray production. Observationally, these systems tend to be radio sources and their X-ray spectra contain a significant non-thermal component. Physically, while the nature of the compact object in LS I +61°303 is still uncertain, PSR B1259–63 contains a rapidly rotating pulsar with a much lower spin period than 1A 0535+262. These two systems present more extreme physical conditions than 1A 0535+262, but equally extreme physical conditions exists in systems which are also undetected in gamma rays. The environmental conditions which lead to gamma-ray production in binary systems remain poorly defined. To more meaningfully constrain theoretical models on gamma-ray production in 1A 0535+262, we would probably need to lower the VHE gamma-ray upper limits by an order of magnitude. This source represents the archetype of the class of Be binary systems which exhibit giant outbursts and the VHE observations were the best we could hope to get in terms of coverage and exposure. The source will be a good target for the next-generation ground-based gamma-ray observatories.

This research is supported by grants from the U.S. Department of Energy, the U.S. National Science Foundation, the Smithsonian Institution, by NSERC in Canada, by Science

Foundation Ireland, and by STFC in the UK. We acknowledge the excellent work of the technical support staff at the FLWO and the collaborating institutions in the construction and operation of the instrument. GM acknowledges support through the Young Investigators Program of the Helmholtz Association. AV and WC wish to acknowledge financial support from NASA and Purdue University.

Facilities: VERITAS, Swift, RXTE, Fermi LAT

REFERENCES

- Abdo, A. A., et al. (Fermi LAT collaboration) 2010a, ApJ, 712, 459
- Abdo, A. A., et al. (Fermi LAT collaboration) 2010b, ApJ, 720, 272
- Abdo, A. A. et al. (Fermi LAT collaboration) 2010c, ApJS, 188, 405
- Acciari, V.A. et al. (VERITAS collaboration) 2008, ApJ, 679, 1427
- Acciari, V.A. et al. (VERITAS collaboration) 2009, ApJ, 698, L94
- Aharonian, F. et al. (H.E.S.S. collaboration) 2004, A&A, 469, L1
- Aharonian, F. et al. (H.E.S.S. collaboration) 2005a, A&A, 442, 1
- Aharonian, F. et al (H.E.S.S. collaboration) 2005b, A&A, 430, 865
- Albert, J. et al. (MAGIC collaboration) 2006, Science, 312 1771
- Atwood, W.B. et al., 2009, ApJ, 697, 1071
- Bednarek, W. 1993, A&A, 278, 307
- Bednarek, W. 2006, MNRAS, 371, 1737
- Burrows, D. N., et al. 2004, Proc. SPIE, 5165, 201
- Caballero, I., et al. 2007a, A&A, 465, L21
- Caballero, I., Kretschmar, P., Santangelo, A., Segreto, A., Ferrigno, C., & Staubert, R. 2007b, ESA Special Publication, 622, 471
- Caballero, I., et al. 2010, arXiv:1003.2969

- Capalbi, M., Perri, M., Saija, B., Tamburelli, F., & Angelini, L. 2005, The Swift XRT Data Reduction Guide, Tech. Rep. 1.2
- Cheng, K.S. & Ruderman, M. 1989 ApJ, 337, L77
- Cheng, K.S. & Ruderman, M. 1991 ApJ, 373, 187
- Coe, M.J. et al. 2006, MNRAS, 368, 447
- Estulin, I. V., Rakhimov, S. I., Novak, B. L., & Eismont, N. A. 1981, Advances in Space Research, 1, 223
- Finger, M.H., Wilson, R.B. & Harmon, B.A. 1996, ApJ, 459, 288
- Fomin, V. P., Stepanian, A. A., Lamb, R. C., Lewis, D. A., Punch, M., & Weekes, T. C. 1994, Astroparticle Physics, 2, 137
- Giovannelli, F. and & Graziati, L.S. 1992, Space Sci. Rev., 59, 1
- Giovannelli, F. et al. 2007, A&A475, 651
- Grove, J. E., et al. 1995, ApJ, 438, L25
- Helene, O. 1983, Nucl. Instrum. Methods, 212, 319
- Hillas, M. 1985, Proc. of the 19th ICRC (La Jolla, IL), 3, 445
- Hinton, J. et al. 2009, ApJ, 690, L101
- Jahoda, K., Swank, J. H., Giles, A. B., Stark, M. J., Strohmayer, T., Zhang, W., & Morgan, E. H. 1996, Proc. SPIE, 2808, 59
- Jahoda, K., Markwardt, C. B., Radeva, Y., Rots, A. H., Stark, M. J., Swank, J. H., Strohmayer, T. E., & Zhang, W. 2006, ApJS, 163, 401
- Kendziorra, E., et al. 1994, A&A, 291, L31
- Krawczynski, H. et al. 2006, Astroparticle Physics, 25, 380
- Li, T. P., & Ma, Y. Q. 1983, ApJ, 272, 317
- Liu, Q.Z. et al. 2006, A&A, 455, 1165
- Makino, F., et al. 1989, IAU Circ., 4769, 1
- Mattox, J. R., et al. 1996, ApJ, 461, 396

- Naik, S., et al. 2008, ApJ, 672, 516
- Orellana, M. & Romero, G.E. 2005, ApJS, 297, 167
- Orellana, M. et al. 2007, A&A, 465, 703
- Perryman, M.A.C. et al. 1997, A&A, 323, L49
- Reig, P. 2007, MNRAS, 377, 867
- Romero, G.E. et al. 2001, A&A, 376, 599
- Romano, P., et al. 2006, A&A, 456, 509
- Rosenberg, F. D., Eyles, C. J., Skinner, G. K., & Willmore, A. P. 1975, Nature, 256, 628
- Sembay, S., Schwartz, R. A., Orwig, L. E., Dennis, B. R., & Davies, S. R. 1990, ApJ, 351, 675
- Steele, I.A. et al. 1998, MNRAS, 295, L5
- Stella, L., White, N. E., & Rosner, R. 1986, ApJ, 308, 669
- Steiner, J. F., McClintock, J. E., Remillard, R. A., Gou, L., Yamada, S., & Narayan, R. 2010, ApJ, 718, L117
- van Paradijs, J., & McClintock, J. E. 1995, X-ray Binaries, 58
- Wilson-Hodge, C.A. et al. 2010, ATel #2324

Table 1. VERITAS observation log

Date	Observation Time (min)	Elevation Range	N_{tel}	Observing Conditions
2009/12/06	20	78° – 80°	4	moon 80% illuminated
2009/12/07	40	58° – 65°	4	bad weather, moon 70% illuminated
2009/12/09	38	83° – 85°	4	moon 48% illuminated
2009/12/10	176	48° – 84°	4	moon 37% illuminated
2009/12/11	52	56° – 80°	4	-
2009/12/12	40	62° – 65°	4	-
2009/12/15	40	53° – 56°	4	-
2009/12/16	60	65° – 74°	4	-
2009/12/17	60	68° – 75°	4	-
2009/12/18	60	75° – 82°	4	-
2009/12/19	60	61° – 69°	4	-
2009/12/20	60	61° – 70°	4	-
2009/12/21	80	67° – 81°	4	bad weather
2009/12/24	60	59° – 68°	3	-
2009/12/25	60	49° – 58°	4	-
2009/12/26	40	55° – 57°	4	-
2010/01/05	37	76° – 80°	4	-
2010/01/07	60	69° – 76°	4	-
2010/01/09	43	80° – 85°	4	bad weather
2010/01/11	8	68° – 70°	4	-
2010/01/12	60	70° – 78°	4	-
2010/01/14	38	71° – 76°	4	-
2010/01/16	60	73° – 81°	4	-
2010/01/17	60	57° – 65°	4	-
2010/02/05	12	82° – 83°	4	-
2010/02/07	20	77° – 80°	4	-
2010/02/08	40	54° – 62°	4	-
2010/02/10	37	60° – 71°	3/4	-
2010/02/12	60	79° – 84°	4	-
2010/02/16	60	70° – 79°	4	-
2010/02/18	60	72° – 82°	4	moon 89% illuminated
2010/02/20	60	75° – 83°	4	moon 98% illuminated

Note. — Data taken in bad weather or under very bright moonlight conditions (> 50% illumination) have been excluded from the data analysis. The column N_{tel} contains the number of working telescopes, from 3 to 4.

Table 2. Swift/XRT observation log

Obs ID	Start (UT; 2009)	End (UT; 2009)	Exposure Time (sec)	Count Rate ^a (cts s ⁻¹)
Rising portion of X-ray flare (MJD 55166.4 – 55177.6)				
00035066002	2009-12-07 00:25:13	2009-12-08 00:30:00	981	195
00035066005	2009-12-08 22:46:41	2009-12-08 23:03:21	995	227
00035066006	2009-12-09 16:08:26	2009-12-09 16:28:00	1154	239
00035066007	2009-12-10 10:09:54	2009-12-10 16:28:00	983	234
00035066008	2009-12-11 00:33:44	2009-12-11 00:51:00	985	246
00035066009	2009-12-12 00:42:28	2009-12-12 00:59:00	977	151
Falling portion of X-ray flare (MJD 55178.4 – 55193.6)				
00035066010	2009-12-13 00:46:28	2009-12-13 01:03:00	972	228
00035066011	2009-12-14 00:47:31	2009-12-14 01:04:00	962	242
00035066012	2009-12-15 00:52:43	2009-12-15 01:11:00	1083	242
00035066013	2009-12-16 00:40:25	2009-12-16 00:58:00	1050	240
00035066014	2009-12-18 00:50:32	2009-12-18 01:07:00	943	200
00035066015	2009-12-19 01:16:47	2009-12-19 01:33:00	968	177
00035066017	2009-12-21 01:11:21	2009-12-21 01:28:00	992	182
00035066018	2009-12-22 09:13:48	2009-12-22 09:35:00	1252	163
00035066020	2009-12-23 09:26:21	2009-12-23 09:45:00	1105	145
00035066021	2009-12-24 09:24:36	2009-12-24 09:42:00	1029	133
00035066022	2009-12-25 08:11:28	2009-12-25 08:31:00	1123	98
00035066023	2009-12-26 08:14:49	2009-12-26 08:35:00	1199	109
00035066024	2009-12-27 08:21:56	2009-12-27 08:41:00	1137	103

^aBackground-subtracted count rates in the 0.6–10.0 keV band. They are not pile-up corrected.

Table 3. RXTE/PCA observation log

Event ID	Start Time (UT)	Stop Time (UT)	Exposure Time (sec)
Rising portion of X-ray flare (MJD 55166.4 – 55177.6)			
94323-04-01-01	2009-12-04 10:27:12	2009-12-04 11:23:44	2448
94323-04-01-00	2009-12-05 16:14:24	2009-12-05 17:58:40	3152
94323-04-01-02	2009-12-06 12:36:32	2009-12-06 13:46:56	3200
94323-04-01-03	2009-12-07 13:45:20	2009-12-07 14:57:36	3232
94323-04-01-04	2009-12-08 14:45:36	2009-12-08 15:55:28	2896
94323-04-01-05	2009-12-09 17:25:20	2009-12-09 18:48:32	3120
94323-04-01-06	2009-12-10 16:55:12	2009-12-10 21:27:28	9952
94323-04-02-00	2009-12-11 11:57:20	2009-12-11 12:59:28	2832
94323-04-02-01	2009-12-12 13:04:16	2009-12-12 14:33:36	2944
Falling portion of X-ray flare (MJD 55178.4 – 55193.6)			
94323-04-02-02	2009-12-13 07:55:12	2009-12-13 08:42:40	2064
94323-04-02-04	2009-12-14 18:29:20	2009-12-14 19:41:36	3376
94323-05-01-00	2009-12-15 14:36:16	2009-12-15 16:05:36	3392
94323-05-01-01	2009-12-16 11:22:24	2009-12-16 12:28:32	3328
94323-05-01-02	2009-12-17 15:14:24	2009-12-17 16:46:40	3392
94323-05-02-03	2009-12-18 14:50:24	2009-12-18 16:30:40	3328
94323-05-02-00	2009-12-19 09:22:24	2009-12-19 13:03:28	6864
94323-05-02-06	2009-12-19 14:25:20	2009-12-19 17:27:28	6720
94323-05-02-04	2009-12-20 12:26:24	2009-12-20 15:35:28	6624
94323-05-02-01	2009-12-21 07:46:24	2009-12-21 10:25:36	4528
94323-05-02-02	2009-12-23 11:03:12	2009-12-23 15:54:40	9920
94323-05-02-05	2009-12-24 10:59:40	2009-12-24 14:50:40	7664
94323-05-03-00	2009-12-25 15:27:28	2009-12-25 16:32:48	2704
94323-05-03-01	2009-12-26 11:26:24	2009-12-26 16:03:44	9072
94323-05-03-02	2009-12-27 14:29:36	2009-12-27 15:34:40	9920
94323-05-03-03	2009-12-28 17:19:28	2009-12-28 19:32:32	3328
Apastron (MJD 55199.4 – 55216.6)			
94323-05-04-00	2010-01-02 01:51:12	2010-01-02 03:31:28	2832
94323-05-04-01	2010-01-04 00:58:24	2010-01-04 02:15:28	3136
94323-05-04-02	2010-01-07 02:36:16	2010-01-07 03:56:32	3008

Table 4. VERITAS Analysis Results

Period	MJD Range	Observation Time (min)	Elevation Range	On Events	Off Events	alpha	Excess Events	Significance (σ)	Flux Upper Limit ($10^{-12} \text{ cm}^{-2} \text{ s}^{-1}$)
All	57166 – 55249	1420	48° – 85°	86	801	0.13	-15.8	-1.5	0.5
Rising portion	55166 – 55178	305	48° – 85°	19	184	0.13	-4.5	-0.9	1.3
Falling portion	55178 – 55193	501	49° – 78°	33	343	0.13	-10.7	-1.6	0.9
Apastron	55199 – 55216	323	57° – 81°	16	161	0.13	-4.5	-1.0	1.0
Periastron	55230 – 55249	289	54° – 85°	18	113	0.13	3.7	0.9	2.0

Note. — Upper limits ($E > 0.3 \text{ TeV}$) are given at 99% confidence level (after Helene (1983)). Significances are calculated using equation (17) from Li & Ma (1983).

Table 5. Fermi LAT Analysis Results

Period	MJD Range	Exposure Time (sec)	Significance ^a (TS)	Flux Upper Limit ^b ($10^{-8} \text{ cm}^{-2} \text{ s}^{-1}$)
All	55165.9 – 55249.1	3125089	0.0	1.9
Rising portion of X-ray flare	55165.9 – 55177.6	429518	0.0	6.4
Falling portion of X-ray flare	55178.4 – 55193.6	515688	0.3	9.8
Apastron	55199.4 – 55216.6	725252	0.0	6.8
Periastron	55230.4 – 55249.6	667580	0.0	5.0

^aThe definition of the test statistic is given by equation (20) of Mattox et al. (1996).

^bThe upper limits are given at the 99% confidence level, for photon energies above 0.2 GeV.

Table 6. Swift/XRT Spectral Results

Obs ID	N_H (10^{22} cm $^{-2}$)	kT_{bb} (keV)	N_{bb} ^a	Γ	N_Γ ^b	χ^2_ν/ν
Rising portion of X-ray flare (MJD 55166.4 – 55177.6)						
00035066002	$0.3^{+0.1}_{-0.1}$	$2.2^{+0.2}_{-0.3}$	$0.2^{+0.1}_{-0.1}$	$0.9^{+0.4}_{-0.2}$	$0.2^{+0.1}_{-0.1}$	1.04/536
00035066005	$0.3^{+0.1}_{-0.1}$	$2.2^{+0.1}_{-0.1}$	$0.3^{+0.1}_{-0.1}$	$1.2^{+0.4}_{-0.3}$	$0.7^{+0.2}_{-0.1}$	1.05/513
00035066006	$0.3^{+0.1}_{-0.1}$	$2.4^{+0.2}_{-0.3}$	$0.2^{+0.1}_{-0.1}$	$1.0^{+0.2}_{-0.2}$	$1.0^{+0.2}_{-0.2}$	1.06/540
00035066007	$0.8^{+0.4}_{-0.3}$	$2.3^{+0.4}_{-0.7}$	$0.2^{+0.2}_{-0.2}$	$0.8^{+0.4}_{-0.3}$	$1.0^{+0.2}_{-0.2}$	1.19/545
00035066008	$0.3^{+0.1}_{-0.1}$	$2.4^{+0.6}_{-1.3}$	$0.2^{+0.3}_{-0.1}$	$0.6^{+0.5}_{-0.2}$	$1.0^{+0.2}_{-0.2}$	1.13/513
00035066009	$0.3^{+0.2}_{-0.1}$	$2.2^{+0.5}_{-0.4}$	$0.2^{+0.2}_{-0.1}$	$0.6^{+0.4}_{-0.2}$	$0.9^{+0.3}_{-0.2}$	1.10/526
Falling portion of X-ray flare (MJD 55178.4 – 55193.6)						
00035066010	$0.1^{+0.2}_{-0.1}$	$2.0^{+0.3}_{-0.3}$	$0.2^{+0.1}_{-0.1}$	$0.7^{+0.6}_{-0.3}$	$0.6^{+0.4}_{-0.2}$	1.11/330
00035066011	$0.2^{+0.4}_{-0.1}$	$2.5^{+0.5}_{-0.9}$	$0.2^{+0.3}_{-0.1}$	$0.7^{+0.8}_{-0.5}$	$0.9^{+0.7}_{-0.4}$	1.05/488
00035066012	$0.2^{+0.1}_{-0.1}$	$2.2^{+0.1}_{-0.2}$	$0.4^{+0.1}_{-0.1}$	$1.1^{+0.3}_{-0.4}$	$0.8^{+0.3}_{-0.2}$	1.01/517
00035066013	$0.3^{+0.2}_{-0.1}$	$2.2^{+0.1}_{-0.2}$	$0.3^{+0.1}_{-0.1}$	$1.1^{+0.4}_{-0.3}$	$0.9^{+0.5}_{-0.2}$	1.07/550
00035066014	$0.5^{+0.2}_{-0.2}$	$2.4^{+0.1}_{-0.1}$	$0.38^{+0.03}_{-0.06}$	$1.8^{+0.6}_{-0.6}$	$1.4^{+1.0}_{-0.6}$	0.99/491
00035066015	$0.4^{+0.2}_{-0.1}$	$2.0^{+0.1}_{-0.1}$	$0.19^{+0.03}_{-0.04}$	$1.6^{+0.5}_{-0.4}$	$1.0^{+0.6}_{-0.3}$	1.07/506
00035066017	$0.4^{+0.1}_{-0.1}$	$2.1^{+0.2}_{-0.2}$	$0.2^{+0.1}_{-0.1}$	$1.2^{+0.4}_{-0.4}$	$0.9^{+0.3}_{-0.4}$	0.97/528
00035066018	$0.3^{+0.1}_{-0.1}$	$2.1^{+0.2}_{-0.3}$	$0.1^{+0.1}_{-0.1}$	$0.9^{+0.4}_{-0.2}$	$0.7^{+0.2}_{-0.1}$	1.13/547
00035066020	$0.5^{+0.3}_{-0.2}$	$2.2^{+0.1}_{-0.3}$	$0.16^{+0.04}_{-0.07}$	$1.4^{+0.7}_{-0.5}$	$0.8^{+0.7}_{-0.3}$	1.15/361
00035066021	$0.2^{+0.2}_{-0.1}$	$1.8^{+0.8}_{-0.2}$	$0.09^{+0.03}_{-0.02}$	$0.9^{+0.4}_{-0.3}$	$0.3^{+0.2}_{-0.1}$	1.05/369
00035066022	$0.2^{+0.1}_{-0.1}$	$1.7^{+0.1}_{-0.1}$	$0.07^{+0.02}_{-0.01}$	$1.1^{+0.5}_{-0.3}$	$0.2^{+0.1}_{-0.1}$	0.90/407
00035066023	$1.0^{+0.1}_{-0.1}$	$1.7^{+0.2}_{-0.1}$	$0.06^{+0.01}_{-0.01}$	$0.7^{+0.3}_{-0.2}$	$0.20^{+0.07}_{-0.04}$	1.02/489
00035066024	$0.2^{+0.3}_{-0.2}$	$1.7^{+0.1}_{-0.1}$	$0.07^{+0.03}_{-0.01}$	$0.7^{+0.4}_{-0.1}$	$0.3^{+0.3}_{-0.1}$	1.13/333

Note. — The columns are: hydrogen column density (N_H), blackbody temperature (T_{bb}), blackbody normalization (N_{bb}), photon index (Γ), power-law normalization (N_Γ), reduced χ^2_ν and degrees of freedom ν .

^aIn units of erg s $^{-1}$ kpc $^{-2}$

^bIn units of ph cm $^{-2}$ s $^{-1}$ keV $^{-1}$

Table 7. RXTE/PCA Spectral Results

Observation ID	kT_{bb} (keV)	N_{bb}^a	kT_s (keV)	kT_e (keV)	τ	N_{comp}	χ^2_ν/ν
Rising portion of X-ray flare (MJD 55166.4 – 55177.6)							
94323-04-01-01	2.0 ^{+0.3} _{-0.2}	0.03 ^{+0.01} _{-0.01}	0.4 ^{+0.2} _{-0.4}	6.3 ^{+0.3} _{-0.2}	8.1 ^{+0.6} _{-0.5}	0.4 ^{+0.7} _{-0.4}	0.41/40
94323-04-01-00	2.3 ^{+0.8} _{-0.3}	0.04 ^{+0.02} _{-0.01}	0.3 ^{+0.4} _{-0.3}	6.5 ^{+0.6} _{-0.2}	7.9 ^{+0.6} _{-0.7}	0.7 ^{+1.1} _{-0.2}	0.23/40
94323-04-01-02	2.8 ^{+1.2} _{-0.6}	0.07 ^{+0.11} _{-0.02}	0.6 ^{+1.1} _{-0.6}	6.7 ^{+1.3} _{-0.4}	7.7 ^{+0.9} _{-1.6}	0.6 ^{+1.4} _{-0.1}	0.22/40
94323-04-01-03	2.3 ^{+0.6} _{-0.3}	0.08 ^{+0.03} _{-0.01}	0.3 ^{+0.4} _{-0.3}	6.5 ^{+0.3} _{-0.2}	8.6 ^{+0.7} _{-0.7}	1.0 ^{+1.3} _{-0.2}	0.23/40
94323-04-01-04	2.3 ^{+0.6} _{-0.2}	0.09 ^{+0.02} _{-0.01}	0.3 ^{+0.3} _{-0.3}	6.5 ^{+0.4} _{-0.2}	9.0 ^{+0.8} _{-0.8}	1.0 ^{+1.3} _{-0.1}	0.28/40
94323-04-01-05	2.2 ^{+0.4} _{-0.2}	0.09 ^{+0.01} _{-0.02}	0.4 ^{+0.3} _{-0.4}	6.4 ^{+0.3} _{-0.2}	9.3 ^{+0.7} _{-0.7}	1.2 ^{+1.3} _{-0.1}	0.16/40
94323-04-01-06	2.2 ^{+0.4} _{-0.2}	0.09 ^{+0.01} _{-0.02}	0.4 ^{+0.2} _{-0.4}	6.4 ^{+0.3} _{-0.2}	9.3 ^{+0.7} _{-0.7}	1.1 ^{+1.2} _{-0.1}	0.16/40
94323-04-02-00	2.3 ^{+0.4} _{-0.2}	0.09 ^{+0.02} _{-0.02}	0.4 ^{+0.2} _{-0.4}	6.5 ^{+0.3} _{-0.2}	9.1 ^{+0.7} _{-0.7}	1.1 ^{+1.4} _{-0.1}	0.25/40
94323-04-02-01	2.4 ^{+0.7} _{-0.3}	0.10 ^{+0.04} _{-0.02}	0.4 ^{+0.2} _{-0.4}	6.5 ^{+0.5} _{-0.2}	9.0 ^{+0.7} _{-0.8}	1.2 ^{+1.5} _{-0.2}	0.22/40
Falling portion of X-ray flare (MJD 55178.4 – 55193.6)							
94323-04-02-02	2.3 ^{+0.5} _{-0.2}	0.10 ^{+0.02} _{-0.02}	0.4 ^{+0.2} _{-0.4}	6.5 ^{+0.3} _{-0.2}	9.3 ^{+0.7} _{-0.7}	1.2 ^{+1.4} _{-0.1}	0.25/40
94323-04-02-04	2.3 ^{+0.5} _{-0.2}	1.10 ^{+0.02} _{-0.02}	0.4 ^{+0.2} _{-0.4}	6.5 ^{+0.4} _{-0.2}	9.2 ^{+0.7} _{-0.7}	1.2 ^{+1.4} _{-0.3}	0.26/40
94323-05-01-00	2.2 ^{+0.4} _{-0.2}	0.09 ^{+0.01} _{-0.01}	0.4 ^{+0.2} _{-0.4}	6.4 ^{+0.2} _{-0.2}	9.4 ^{+0.7} _{-0.7}	1.1 ^{+1.3} _{-0.1}	0.22/40
94323-05-01-01	2.2 ^{+0.6} _{-0.2}	0.08 ^{+0.01} _{-0.01}	0.4 ^{+0.2} _{-0.4}	6.4 ^{+0.3} _{-0.2}	9.2 ^{+0.6} _{-0.8}	1.1 ^{+1.3} _{-0.1}	0.24/40
94323-05-01-02	2.3 ^{+0.6} _{-0.3}	0.08 ^{+0.02} _{-0.01}	0.4 ^{+0.3} _{-0.4}	6.4 ^{+0.4} _{-0.2}	9.1 ^{+0.8} _{-0.8}	1.1 ^{+1.3} _{-0.1}	0.24/40
94323-05-02-03	2.2 ^{+0.4} _{-0.2}	0.07 ^{+0.01} _{-0.01}	0.4 ^{+0.2} _{-0.4}	6.4 ^{+0.3} _{-0.2}	9.2 ^{+0.7} _{-0.7}	0.9 ^{+1.2} _{-0.1}	0.22/40
94323-05-02-00	2.2 ^{+0.4} _{-0.2}	0.07 ^{+0.10} _{-0.01}	0.4 ^{+0.3} _{-0.4}	6.4 ^{+0.3} _{-0.2}	9.0 ^{+0.7} _{-0.6}	0.9 ^{+1.1} _{-0.1}	0.15/40
94323-05-02-06	2.2 ^{+0.6} _{-0.2}	0.06 ^{+0.01} _{-0.01}	0.4 ^{+0.2} _{-0.4}	6.4 ^{+0.2} _{-0.2}	8.9 ^{+0.7} _{-0.6}	0.9 ^{+1.2} _{-0.1}	0.20/40
94323-05-02-04	2.1 ^{+0.5} _{-0.2}	0.05 ^{+0.01} _{-0.01}	0.3 ^{+0.4} _{-0.3}	6.4 ^{+0.3} _{-0.2}	8.9 ^{+0.7} _{-0.7}	0.9 ^{+1.1} _{-0.1}	0.17/40
94323-05-02-01	2.1 ^{+0.4} _{-0.2}	0.05 ^{+0.01} _{-0.01}	0.4 ^{+0.3} _{-0.4}	6.4 ^{+0.3} _{-0.2}	8.9 ^{+0.6} _{-0.5}	0.8 ^{+1.0} _{-0.1}	0.14/40
94323-05-02-02	2.1 ^{+0.5} _{-0.2}	0.04 ^{+0.08} _{-0.07}	0.3 ^{+0.3} _{-0.3}	6.4 ^{+0.3} _{-0.2}	8.4 ^{+0.6} _{-0.5}	0.7 ^{+1.0} _{-0.1}	0.15/40
94323-05-02-05	2.1 ^{+0.4} _{-0.2}	0.03 ^{+0.01} _{-0.01}	0.4 ^{+0.3} _{-0.4}	6.4 ^{+0.3} _{-0.2}	8.4 ^{+0.6} _{-0.5}	0.6 ^{+0.9} _{-0.1}	0.17/40
94323-05-03-00	2.1 ^{+0.5} _{-0.2}	0.03 ^{+0.01} _{-0.01}	0.3 ^{+0.4} _{-0.3}	6.4 ^{+0.3} _{-0.2}	8.4 ^{+0.7} _{-0.6}	0.6 ^{+0.9} _{-0.1}	0.30/40
94323-05-03-01	2.0 ^{+0.3} _{-0.1}	0.03 ^{+0.01} _{-0.01}	0.4 ^{+0.2} _{-0.4}	6.2 ^{+0.2} _{-0.1}	8.5 ^{+0.5} _{-0.5}	0.44 ^{+0.73} _{-0.04}	0.20/40
94323-05-03-02	2.0 ^{+0.4} _{-0.2}	0.01 ^{+0.01} _{-0.01}	0.4 ^{+0.3} _{-0.4}	6.2 ^{+0.3} _{-0.2}	8.3 ^{+0.7} _{-0.5}	0.4 ^{+0.6} _{-0.1}	0.20/40
94323-05-03-03	2.0 ^{+0.4} _{-0.2}	0.02 ^{+0.01} _{-0.01}	0.3 ^{+0.4} _{-0.3}	6.1 ^{+0.3} _{-0.2}	8.2 ^{+0.7} _{-0.6}	0.4 ^{+0.6} _{-0.1}	0.20/40
Apastron (MJD 55199.4 – 55216.6)							
94323-05-04-00	1.9 ^{+0.4} _{-0.2}	0.007 ^{+0.002} _{-0.002}	0.4 ^{+0.2} _{-0.4}	6.3 ^{+0.4} _{-0.2}	6.9 ^{+0.5} _{-0.5}	0.15 ^{+0.43} _{-0.02}	0.61/40
94323-05-04-01	1.8 ^{+0.7} _{-0.2}	0.004 ^{+0.002} _{-0.001}	0.4 ^{+0.3} _{-0.4}	6.4 ^{+0.7} _{-0.4}	6.3 ^{+0.6} _{-0.7}	0.09 ^{+0.13} _{-0.02}	0.61/40
94323-05-04-02	2.6 ^{+1.2} _{-1.0}	0.002 ^{+0.001} _{-0.001}	0.6 ^{+0.1} _{-0.6}	3.4 ^{+2.3} _{-1.2}	3.6 ^{+1.7} _{-2.5}	0.2 ^{+0.1} _{-0.2}	0.67/40

Note. — The parameters for the Compton component are: seed photon temperature (T_s), electron temperature (T_e), optical depth (τ), and normalization (N_{comp}). The geometry parameter is frozen at 0.8, and N_H is fixed at $0.3 \times 10^{22} \text{cm}^{-2}$.

^aIn units of $\text{erg s}^{-1} \text{kpc}^{-2}$

Table 8: Joint Swift/RXTE Spectral Fits

	N_H 10^{22}cm^{-2}	Swift			RXTE			τ	N_{comp}	χ^2_ν/ν
		kT_{bb} (keV)	N_{bb}^\dagger	kT_{bb} (keV)	N_{bb}^\dagger	kT_s (keV)	kT_e (keV)			
<i>Rising portion</i>	$0.34^{+0.01}_{-0.02}$	$1.95^{+0.06}_{-0.07}$	$0.27^{+0.01}_{-0.03}$	$2.02^{+0.16}_{-0.12}$	$0.08^{+0.02}_{-0.02}$	$0.11^{+0.05}_{-0.11}$	$6.3^{+0.2}_{-0.1}$	$9.5^{+0.6}_{-0.5}$	$1.20^{+0.83}_{-0.10}$	$1.18/851$
	$0.33^{+0.01}_{-0.01}$		$1.65^{+0.03\dagger}_{-0.03}$	$0.168^{+0.007\dagger}_{-0.006}$		$0.132^{+0.04}_{-0.13}$	$5.87^{+0.07}_{-0.07}$	$12.31^{+0.2}_{-0.6}$	$1.6^{+0.7}_{-0.1}$	$1.44/853$
<i>Falling portion</i>	$0.33^{+0.01}_{-0.01}$	$1.94^{+0.05}_{-0.04}$	$0.118^{+0.006}_{-0.006}$	$2.33^{+0.58}_{-0.26}$	$0.017^{+0.203}_{-0.004}$	$0.06^{+0.18}_{-0.06}$	$6.5^{+0.3}_{-0.2}$	$8.0^{+0.4}_{-0.5}$	$0.5^{+0.3}_{-0.1}$	$1.32/881$
	$0.24^{+0.03}_{-0.03}$		$1.49^{+0.02\dagger}_{-0.02}$	$0.071^{+0.002\dagger}_{-0.002}$		$0.23^{+0.04}_{-0.04}$	$5.67^{+0.05}_{-0.05}$	$12.70^{+0.3}_{-0.4}$	$0.52^{+0.02}_{-0.02}$	$1.78/877$

Note. — The blackbody component is shown for Swift/XRT and RXTE/PCA data separately. The parameters for the Compton component are: seed photon temperature (T_s), electron temperature (T_e), optical depth (τ), and normalization (N_{comp}). The geometry parameter is frozen at 0.8.

[†]In units of $\text{erg s}^{-1} \text{kpc}^{-2}$

[‡]The blackbody temperature kT_{bb} and normalization parameter N_{bb} , respectively, are tied between the Swift and RXTE data.

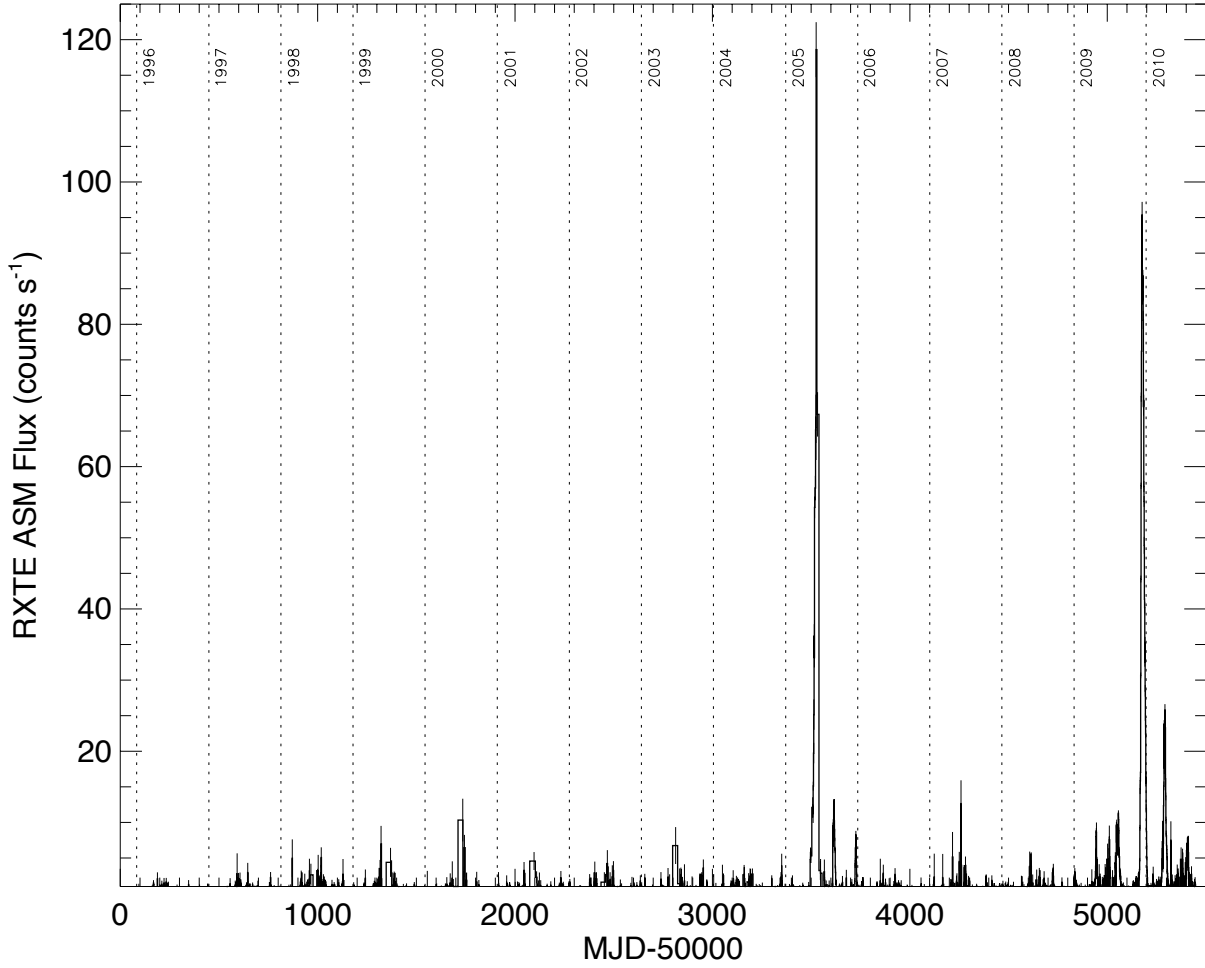


Fig. 1.— Long-term RXTE/ASM (1.5–12 keV) light curve of 1A 0535+262, from 1996 January 5 to 2010 September 9. Note the presence of outbursts of different types.

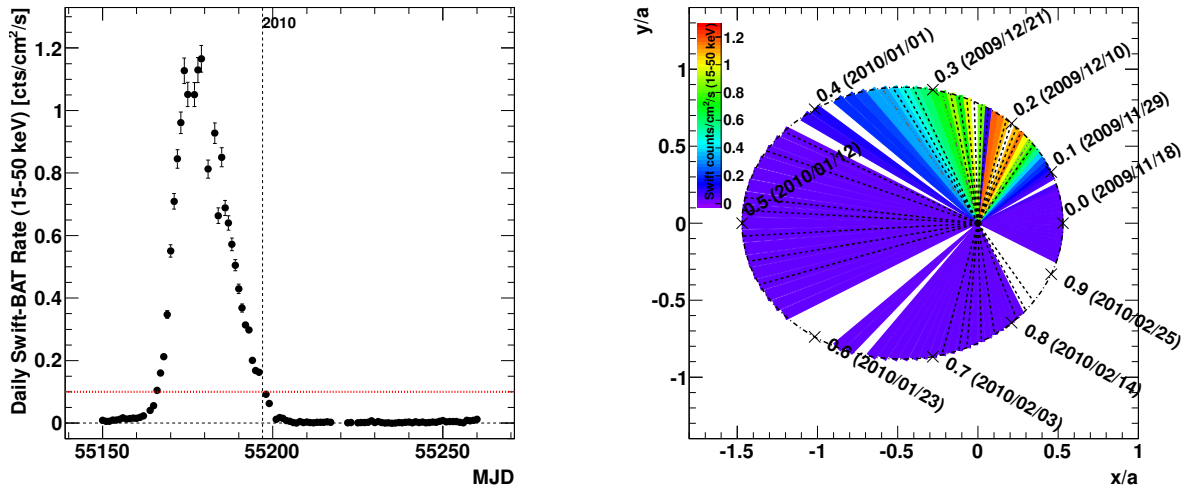


Fig. 2.— Left: Swift/BAT counting rate vs time in the 15-50 keV energy range. The horizontal line at $0.1 \text{ cts/cm}^2/\text{s}$ indicates the trigger threshold for observations with VERITAS. Right: Relative orbit of the neutron star around the Be star. The primary star lies in the focus of the ellipse $(0,0)$ and the axis units are multiples of the semi-major axis of the orbit. The most probably inclination of the binary system is 35 to 39° (Giovannelli et al. 2007). Indicated in colors is the Swift/BAT counting rate in the 15-50 keV energy range for the orbit starting in November 2009. The dashed lines indicate nights with VERITAS observations, covering the flare, apastron, and periods close to periastron. Orbital parameters after Coe et al. (2006).

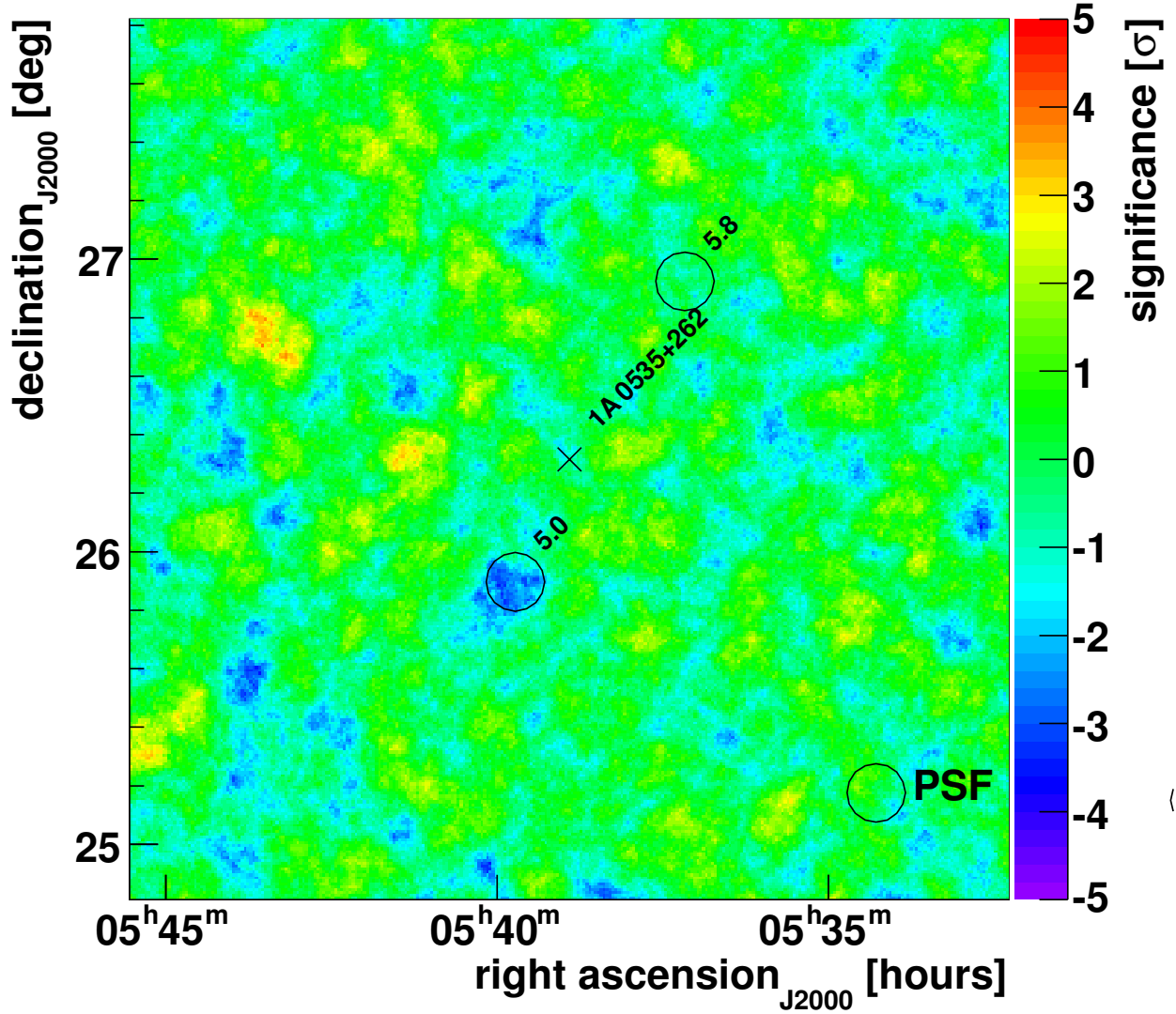


Fig. 3.— VERITAS significance map of the region around 1A 0535+262 in equatorial coordinates for the period MJD 57166-55250. The location of 1A 0535+262 is indicated by a black cross at the center. Also shown are regions excluded from the background calculation due to bright stars. The numbers beside the excluded regions indicate the B magnitude of these stars. The circle at the bottom right indicates the angular resolution of the VERITAS observations.

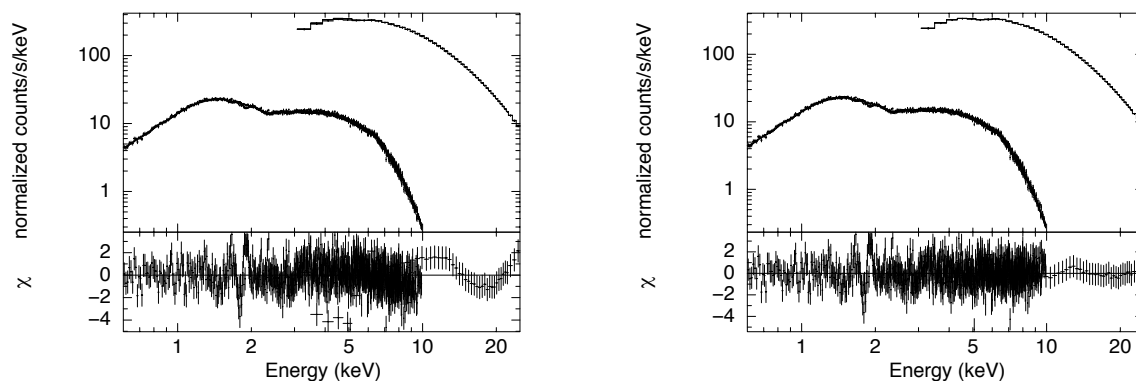


Fig. 4.— Joint Swift/XRT and RXTE/PCA spectral modeling of 1A 0535+262 for the rising portion of the X-ray outburst. The upper panel shows the Swift/XRT data (lower curve) and the RXTE/PCA data (upper curve), and the lower panel shows the residuals of the fit. (*left*) A fit to the data with a model that consists of blackbody radiation and thermal Comptonization, with all physical parameters tied for the XRT and PCA data sets. Note a significant pattern in the residuals of the fit (shown in the bottom panel) in the PCA band. (*right*) A fit to the data with the same model but with the blackbody temperature and normalization untied between the two data sets.